https://doi.org/10.5194/egusphere-2025-1458
Preprint. Discussion started: 14 April 2025

Meteorological Landscape of Tropical Cyclone

Pascal Oettli[1], Keita Tokuda[2], Yusuke Imoto[3], Shunji Kotsuki[4,1,5]

[1]Center of Environmental Remote Sensing, Chiba University, 1-33, Yayoi-cho, Inage-ku, Chiba, 263-8522, Japan
[2]Faculty of Health Data science, Juntendo University, 6-8-1, Hinode-cho, Urayasu, Chiba, 279-0013, Japan
[3]Institute for the Advanced Study of Human Biology, Kyoto University, Yoshida Konoe-cho, Sakyo-ku, Kyoto, 606-8501, Japan
[4]Institute for Advanced Academic Research, Chiba University, 1-33, Yayoi-cho, Inage-ku, Chiba, 263-8522, Japan
[5]Research Institute of Disaster Medicine, Chiba University, 1-8-1, Inohana, Chuo-ku, Chiba, 260-0856, Japan

Correspondence to: Pascal Oettli (oettli@chiba-u.jp), Shunji Kotsuki (shunji.kotsuki@chiba-u.jp), and Yusuke Imoto (imoto.yusuke.4e@kyoto-u.ac.jp)

Abstract. A tropical cyclone is a meteorological phenomenon that produces heavy rainfall, damaging winds, thunderstorms, storm surges, among others. This is also a system of complex interactions between local sea-surface temperatures vertical atmospheric conditions, such as shear winds, and regional steering flows. A single discipline cannot rise to the challenge posed by the understanding of the mechanisms governing the birth, maturity, and decay of a tropical cyclone. Collaborative work between earth science and other disciplines can address such a challenge, by offering new angles of thinking and new techniques of research to apprehend such a complex phenomenon. In this study, we apply biological concepts such as the Waddington's epigenetic landscape, and bioinformatics techniques like the graph-Hodge decomposition, to meteorology, to introduce an innovative way to characterize the evolution of three tropical cyclones: "Dolphin," "Nepartak," and "Meari". When applied to an ensemble prediction system, the result is a meteorological landscape depicting the creodes reflecting possible paths and their associated probabilities of realization.

1 Introduction

Tropical cyclone (TC) is an extreme weather event, which can become a major disaster when approaching lands, because it generates intense winds, heavy rains, and coastal surges. It is, therefore, a threat to human life, notably because of floodings and landslides. It is also causing important damage, social disruption, economic and environmental costs. Over the past 40 years (1979–2019), 1.945 TC-related disasters have been identified worldwide (WMO, 2021) and held responsible for the death of 779.324 people and the economic loss of US$ 1.4 trillion (WMO, 2021). In Japan only, 101 TC-related disasters generated a total economic loss of US$ 136.03 billion (WMO, 2021). In meteorological phenomena, including TCs, trajectories sometimes appear to split into multiple distinct states with time, typically evolving into disaster (i.e., flooding, storm surge, landslides...) and non-disaster states. It is then important to know in advance the future evolution of an extreme weather event, particularly the likelihood of a disaster state. A tropical cyclone approaching land increases the probability of a disaster, to the contrary of a further offshore position. To support disaster prevention, it is essential to know in advance

https://doi.org/10.5194/egusphere-2025-1458
Preprint. Discussion started: 14 April 2025

when plausible scenarios start to distinguish one from the others, requiring the development of early detection methods. Ensemble prediction system (EPS) has been used to provide scenarios of evolutions that are possible, via its ensemble members (EM), because the future state of the atmosphere predicted by a single EM is considered to be less important than the estimate of the future probability density from all the EMs (Leutbecher and Palmer, 2008). Also, it is generally admitted that the average of all EMs provides a more accurate estimation for TC's track and intensity than a single forecast. Beyond the simple arithmetic average, selective ensemble-mean methods applied on multi-ensemble tracks has been proven to reduce the forecast errors, for example by weighting the average according to the EM position error (Nishimura and Yamaguchi, 2015) or by retaining the most populated cluster (Kowaleski and Evans, 2020).

Because of the initial perturbations used to produce the ensemble members, it is not rare for an EPS to forecast more than one scenario at a given initialization time, with groups of tracks parting away from each other (Fig. 1b). The two groups "Western TCs" (dark magenta) and "Eastern TCs" (strong blue) can thus be considered as two different modes of behaviour diverging from an initial state (orange left right arrow). The groups of tracks are spatially separated by a boundary (red dashed line).

By analogy to developmental biology (Fig. 1a), the two modes of behaviour can be seen as two pathways (or creodes), with two states of terminal differentiation or attractors, valid for the given initialization time and only for it. The point where the spatial divergence could then be called a bifurcation and the spatial boundary a separatrix. Furthermore, these components put together with a changing potential surface (Thom, 1975) define the so-called Waddington's epigenetic landscape, named from Conrad Hal Waddington (Waddington, 1957), which is a metaphor of a single-cell trajectory during its differentiation (Ferrell, 2012; Gilbert, 1991).

https://doi.org/10.5194/egusphere-2025-1458
Preprint. Discussion started: 14 April 2025

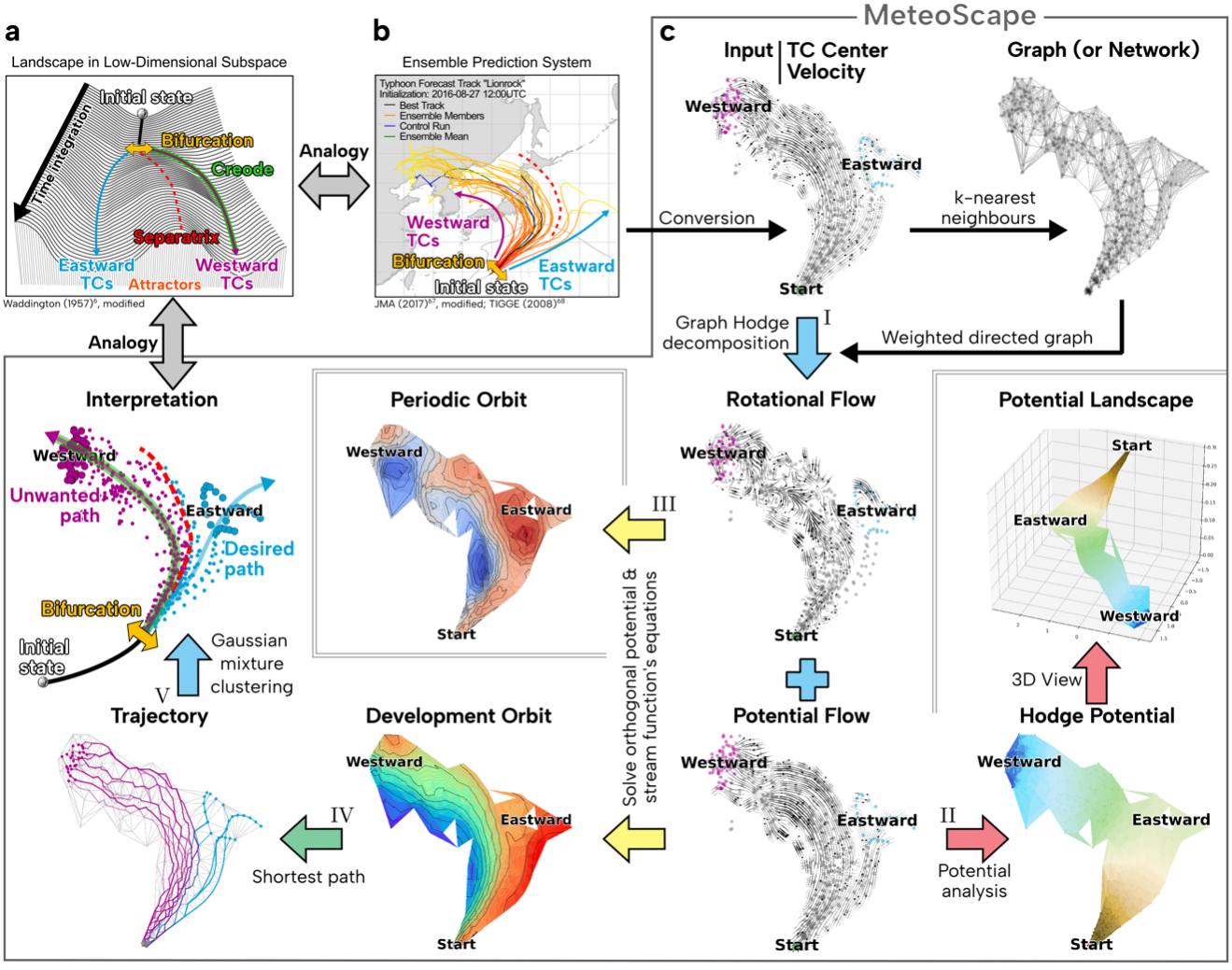

Figure 1: Overview of MeteoScape. Analogy between a) mathematical research and b) ensemble prediction system (tropical cyclone "Lionrock"). c) the different steps of the MeteoScape, from the graph Hodge decomposition (I), through potential analysis (II) equation solving (III) and shortest path (IV), to the Gaussian mixture clustering (IV), The final product is the meteorological landscape. Ensemble Prediction System figure is adapted from JMA (2017) and Landscape in Low-Dimensional Subspace is adapted from Waddington (1957). TC "Lionrock" tracks are extracted from THORPEX Interactive Grand Global Ensemble (TIGGE) Model Tropical Cyclone Track Data (National Centers for Environmental Prediction/National Weather Service/NOAA/U.S. Department of Commerce et al., 2008).

In the classic visualization of the Waddington's model (Ferrell, 2012; Gilbert, 1991; Rossi et al., 2015; Waddington, 1957), the shape of the potential surface forms a landscape of valleys and ridges. Each new "valley" offers an alternative fate to the cell (or any other system), while the "ridges" prevent the system from switching from one fate to another (Slack, 2002). Because it is a dynamical system, computing the potential energy (i.e., the "valleys" and the "ridges") will predict the evolution of the system. Any points of the system can be associated with a vector representing its evolution in time, i.e., change in speed and in direction (Slack, 2002), in the form of a vector field. Here, the vector field consists of the different

https://doi.org/10.5194/egusphere-2025-1458
Preprint. Discussion started: 14 April 2025

positions of a tropical cyclone forecasted by an EPS and the associated vectors are the speed and direction between two consecutive forecast times.

The main objective of this study is to provide a mathematical method to understand the evolution of a tropical cyclone in time through the visualization of the "valleys" and "ridges" in the potential surface. Or more simply, the "Waddington's epigenetic landscape" of the tropical cyclone. Here we hypothesized such landscape exists for tracks of TCs because they are mainly dominated by lateral boundary. In this study, we propose to complete the following tasks, using the information provided by an EPS:

- Calculating the potential surface (i.e., landscape) from the forecasted tracks.
- Detecting the major pathways (i.e., creodes in the Waddington's landscape) in the potential surface.
- Locating the separatrix (i.e., ridges in the landscape) in the potential surface.

2 Materials and Methods

2.1 MeteoScape

We first create an undirected graph from 2D point cloud $X = (x_1, \dots x_n) \in \mathbb{R}^{2\times n}$. We used the k-nearest neighbour (kNN) algorithm (Bentley, 1975; Eppstein et al., 1997), which connects to kNN of the point cloud based on a distance metric, to define edges. Let (V, E) be an undirected graph with $V = X$ and $e_{ij} \in E$ if kNN of x_i includes x_j. In the current work, k=15 (Fig. 2a). Changing this value hardly changes the results presented herewith but has an impact on the computation time.

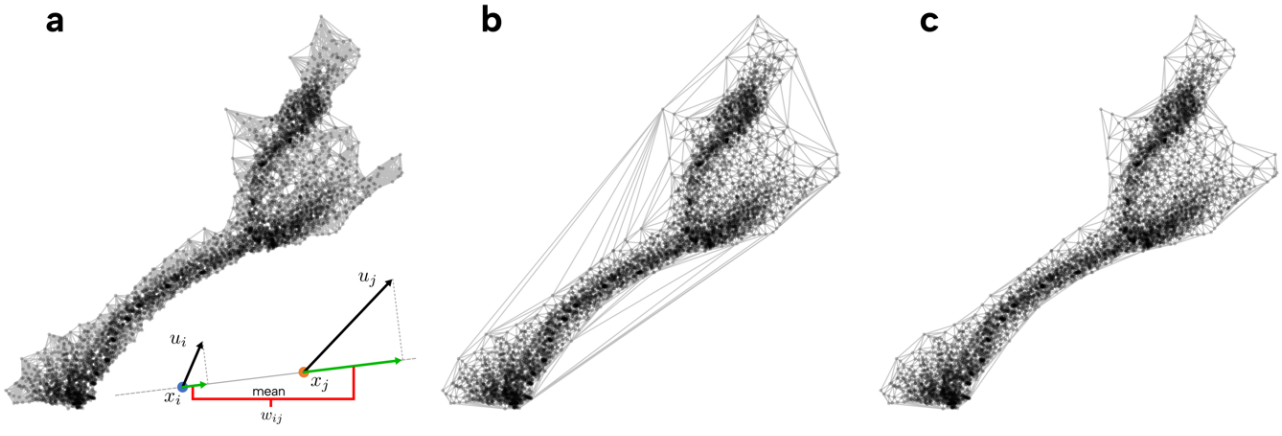

Figure 2: Definition of the graphs. a) k-nearest neighbours (with k=15) applied to the 2D data in Fig. 6d, b) Delaunay triangulation for the same 2D data and c) the final graph after removing the unnecessary edges and triangles. The graph in a) is used to perform the graph Hodge decomposition, while c is used to calculate the shortest paths in b. Inset in a) illustrates the calculation of the embedded velocity between two nodes x_i and x_j (blue and orange dots respectively). First, the velocity vectors u_i and u_j (black arrows) are projected onto the line connecting the nodes (grey long-dashed line) with an orthogonal basis (grey dotted segments) to obtain the projected velocity (green arrows). Second, the mean (in red) of the two projected vectors is calculated to provide the weight w_{ij} of the edge (grey segment).

https://doi.org/10.5194/egusphere-2025-1458
Preprint. Discussion started: 14 April 2025

Next, we create a weighted directed graph to the edge using velocity data $U = (u_1 \dots, u_n) \in \mathbb{R}^{2\times n}$. The weights w_{ij} are calculated by deriving the embedded velocities from the 2D point cloud and velocities (inset in Fig. 2a). Velocity vectors $u(i)$ and $u(j)$ (black arrows) are orthogonally projected onto the edge (grey segment) connected vertices x_i and x_j (coloured dots). The mean of projected velocities (green arrows) is calculated to get the weights assigned to the edges:

$$w_{ij} = \frac{u_i+u_j}{2} \cdot \frac{x_i-x_j}{\|x_i-x_j\|}. \quad (1)$$

The direction of edge is determined by the sign of the weight, i.e., $x_i \to x_j$ if $w_{ij} > 0$, $x_j \to x_i$ if $w_{ij} < 0$, and no arrow between x_i and x_j if $w_{ij} = 0$. We denote the weighted directed graph as $G = (V, E, W)$, where $W = (w_{ij}) \in \mathbb{R}^{|E|}$.

Next, we apply the graph-Hodge decomposition (GHD) to weighted directed graph $G = (V, E, W)$. GHD decomposes weight vector W as

$$W = W^{\mathrm{pot}} + W^{\mathrm{rot}}. \quad (2)$$

Using decomposed weight vectors $W_{\mathrm{pot}}, W_{\mathrm{rot}}$, weighted directed graph $G = (V, E, W)$ is decomposed to $G^{\mathrm{pot}} = (V, E, W^{\mathrm{pot}})$ and $G^{\mathrm{rot}} = (V, E, W^{\mathrm{rot}})$. G^{pot} is acyclic (curl-free) and G^{rot} is a balanced flow rate (divergence-free). In addition, GHD algorithm simultaneously derives potential $\phi: V(= X) \to \mathbb{R}$ satisfying $-\nabla^{\mathrm{G}}\phi = W^{\mathrm{pot}}$ ($\nabla^{\mathrm{G}}: \mathbb{R}^{|E|} \to \mathbb{R}^{|V|}$ is the gradient on weighted directed graph G (Lim, 2020). From these graphs, we can reconstruct the velocity corresponding to the potential and rotational flow:

$$u_i^{\mathrm{pot}} = \frac{1}{|E_i|}\sum_{j\in E_i} w_j^{\mathrm{pot}} \frac{x_i-x_j}{\|x_i-x_j\|} \quad (\mathrm{resp.}\, u_i^{\mathrm{rot}}), \quad (3)$$

where E_i is the index set of nodes connected to node x_i. The contribution rates of potential flow c^{pot} and rotational flow c^{rot} are introduced by

$$c^{\mathrm{pot}} = \frac{\tilde{c}^{\mathrm{pot}}}{\tilde{c}^{\mathrm{pot}}+\tilde{c}^{\mathrm{rot}}}, c^{\mathrm{rot}} = \frac{\tilde{c}^{\mathrm{rot}}}{\tilde{c}^{\mathrm{pot}}+\tilde{c}^{\mathrm{rot}}} \quad (4)$$

With

$$\tilde{c}^{\mathrm{pot}} = \sqrt{\sum_i \left[\mathrm{ReLU}\left(\frac{u_i}{|u_i|} \cdot u_i^{\mathrm{pot}}\right)\right]^2} \quad (\mathrm{resp.}\, \tilde{c}^{\mathrm{rot}}). \quad (5)$$

Here, ReLU is the rectified linear unit, i.e., $\mathrm{ReLU}(\mathrm{x}) = \max(0, \mathrm{x})$. The contribution rates describe the similarity rates to the original flow: The contribution rate of a flow is high when the directions of corresponding velocity are like the original one: if $u_i = u_i^{\mathrm{pot}}$ for all i, $c^{\mathrm{pot}} = 1$ and $c^{\mathrm{rot}} = 0$.

To infer the orbits on the landscape constructed by potential ϕ, we introduce an orthogonal potential. Orthogonal potential ψ is designed as satisfying $\nabla\phi \cdot \nabla\psi = 0$ and $\psi \not\equiv \mathrm{const}$. The contours of ψ correspond to the orbit of $\nabla\phi$. In the 2D case, orthogonal potential ψ can be computed using the orthogonal velocity of u^{pot}. That is, replacing $U = (u_1 \dots, u_n)$ with $U^{\mathrm{pot}\perp} = (u_1^{\mathrm{pot}\perp} \dots, u_n^{\mathrm{pot}\perp})$ defined by

$$u_i^{\mathrm{pot}\perp} = \begin{pmatrix} 0 & -1 \\ 1 & 0 \end{pmatrix} u_i^{\mathrm{pot}}, \quad (6)$$

we compute orthogonal potential ψ following the algorithm above.

https://doi.org/10.5194/egusphere-2025-1458
Preprint. Discussion started: 14 April 2025

We use another graph representation based on the Delaunay triangulation algorithm to infer orbits between two data points. Delauney triangulation is a dual of Voronoi decomposition and generates a triangle mesh for a point cloud. Because of the algorithm, unnecessary triangles and sides tend to be created between distant points, particularly at the bounding envelope (Fig. 2b). Triangles with large volumes are deleted when their areas are larger than the standard deviation of all the areas. Long edges are also cut when their length is longer than the standard deviation of all the side lengths (Fig. 2c). We use the Delaunay-based graph for inferring the orbits because the kNN graph is too dense and the orbits on it are uninterpretable.

We define weights of edges on Delaunay-based graph and detect orbits on the landscape for the pair of points. It is ideal that a particle in the landscape moves on the corresponding contour of orthogonal potential because the contours of orthogonal potential show orbits of potential flow. Therefore, for the start point x_s (source) and end point x_t (target), we define weight $W^{\mathrm{D}} = (w_{ij}^{\mathrm{D}})$ on the edge in the Delaunay graph by

$$w_{ij}^{\mathrm{D}} = \left|\psi(x_t) - \frac{\psi(x_i)+\psi(x_j)}{2}\right| \times \exp\left(\frac{|x_i - x_j|}{\mathrm{mean}_{k<\ell}\{|x_k - x_\ell|\}}\right). \quad (7)$$

The first term is a weight that decreases when the average orthogonal potential of the connecting vertices is close to the orthogonal potential of target x_t. The second term (constant for point cloud X) increases corresponding the length of edges, preventing unnatural shortcuts. Using the weighted Delaunay-based graph, we detect orbit between source x_s and target x_t using Dijkstra's algorithm (Dijkstra, 1959), thus providing an optimal trajectory between x_s and x_t. Because it minimizes the displacement cost between source and target, it is expected that optimal trajectories from the same source but to two different targets to show a clear separation at some point (the saddle point), because it is less costly to move along the development orbit (Fig. 3b) than crossing it. By assigning all the nodes X to one of the targets (Fig. 4a; "Northward" and "Eastward"), it is possible to objectively find the saddle point and to visualize the separatrix.

https://doi.org/10.5194/egusphere-2025-1458
Preprint. Discussion started: 14 April 2025

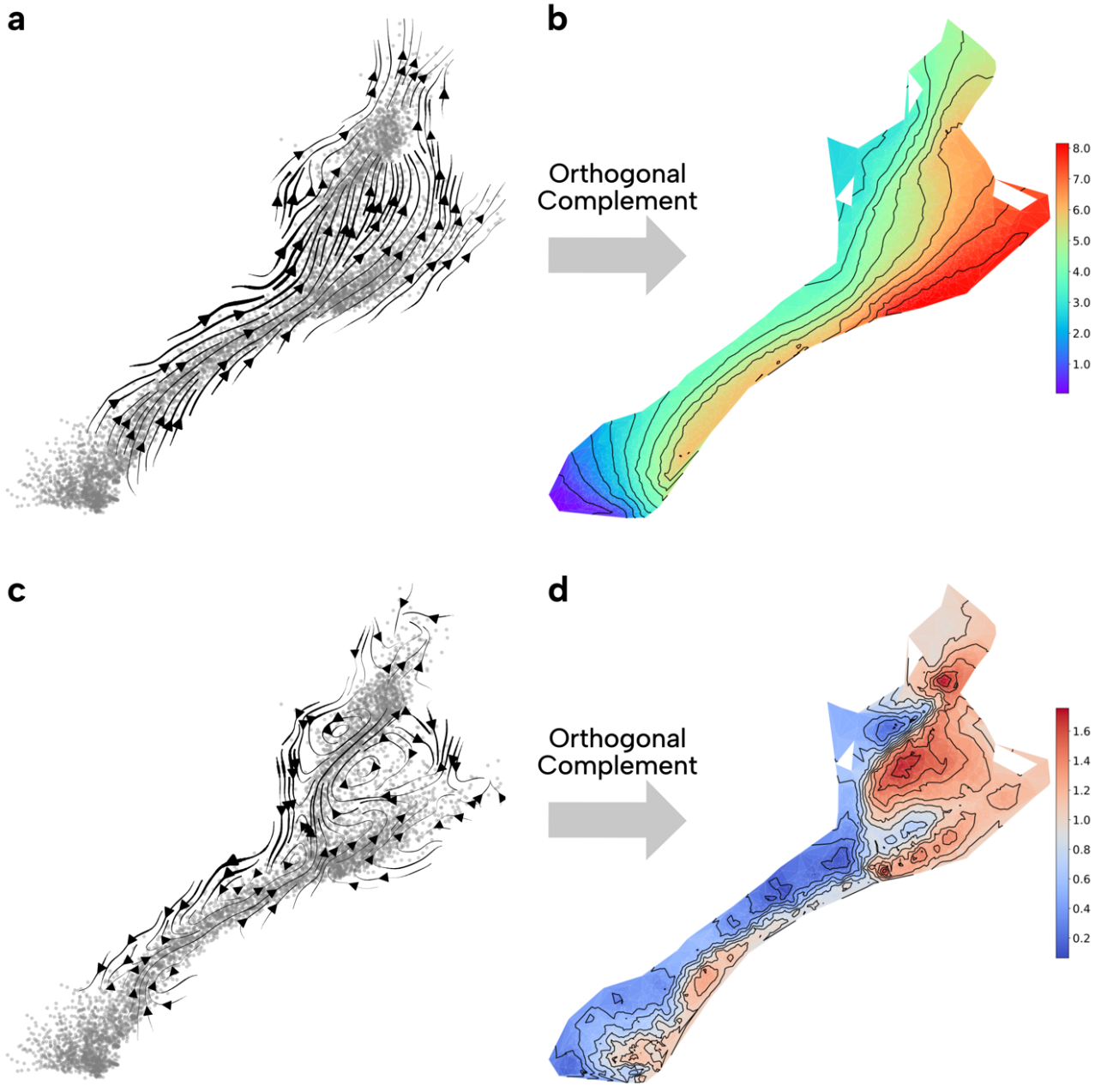

Figure 3: Products of the graph Hodge decomposition and their respective orthogonal component. a) Potential flow ($-\nabla\phi$) (= irrotational vector field) calculated by the graph Hodge decomposition of the input data (Fig. 6 d), and b) its orthogonal complement, the development orbit. c) Rotational flow ($\nabla \times A$) (= solenoidal vector field) calculated by the graph Hodge decomposition of the input data (Fig. 6 d), and d) its orthogonal complement, the periodic orbit.

https://doi.org/10.5194/egusphere-2025-1458
Preprint. Discussion started: 14 April 2025

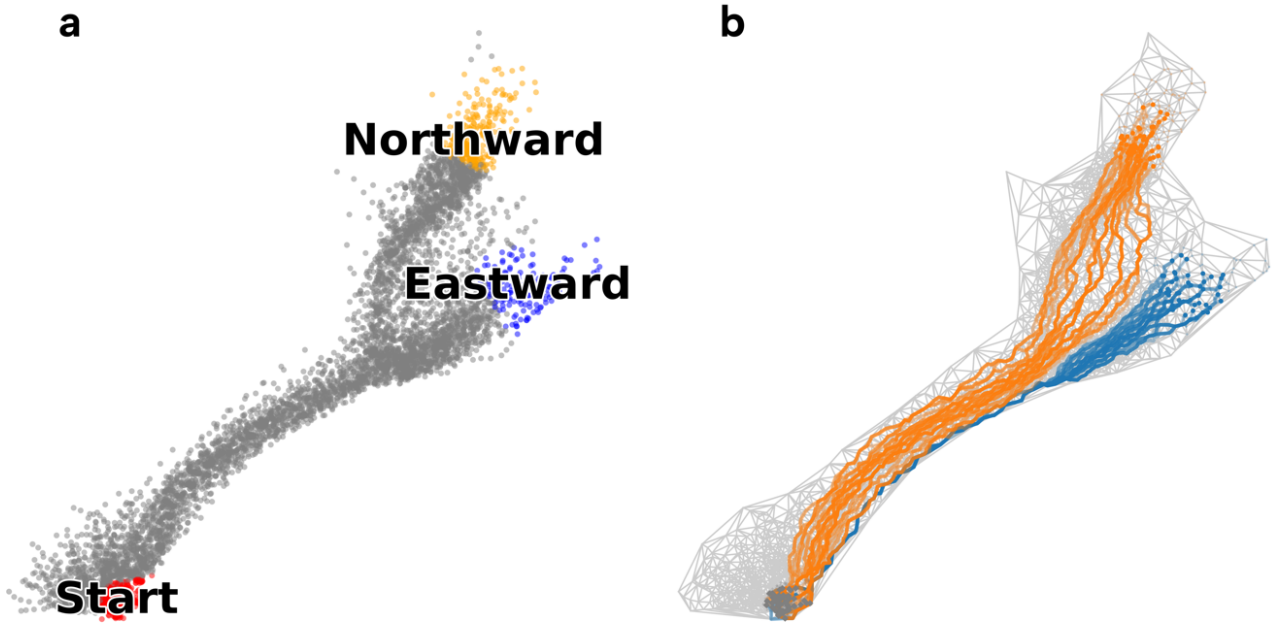

Figure 4: Cluster definition and trajectories from source to targets. a) Definition of the clusters. b) Optimal trajectories based on the shortest path (Dijkstra's algorithm). The weight of the edges is provided by the development orbit (Fig. 3b).

For each target cluster k $(k = 1, \dots, K)$, we first calculate mean μ_k and standard deviation σ_k of orthogonal potential ψ:

$$w_{ij}^{\mathrm{D}} = \left|\psi(x_t) - \frac{\psi(x_i)+\psi(x_j)}{2}\right| \times \exp\left(\frac{|x_i - x_j|}{\mathrm{mean}_{k<\ell}\{|x_k - x_\ell|\}}\right). \quad (8)$$

$$\sigma_k = \sqrt{\frac{1}{|\Lambda_k|}\sum_{i\in\Lambda_k}[\psi(x_i) - \mu_k]^2}, \quad (9)$$

where Λ_k is the index set of nodes belonging to target cluster k. Then we define the probability distribution function D of the Gaussian mixture from the means and standard deviations:

$$D(\psi(x_i)|\mu_k, \sigma_k) = \frac{1}{\sigma_k\sqrt{2\pi}} e^{-\frac{(\psi(x_i)-\mu_k)^2}{2\sigma_k^2}}, \quad (10)$$

where $\psi(x_i)$ is the orthogonal potential at node x_i.

From D we compute the probability P_k of anode x_i to belong to cluster k:

$$P_k(x_i) = w_k D(\psi(x_i)|\mu_k, \sigma_k), \quad (11)$$

where w_k is the weight of cluster k:

$$w_k = \frac{|\Lambda_k|}{\sum_{j=1}^{K}|\Lambda_j|}, \quad (12)$$

where K is the total number of target clusters. In this study, K is always equal to 2. The hyperparameter values are shown in Table 1.

https://doi.org/10.5194/egusphere-2025-1458
Preprint. Discussion started: 14 April 2025

Table 1: Hyper parameters of the Gaussian mixture: Cluster (k), weight (w_k), mean (μ_k) and standard deviation (σ_k), by tropical cyclone.

	Cluster k	Weight w_k	Mean μ_k	Standard deviation σ_k
"Dolphin"	Northward	0.6759	5.7221	0.4503
	Eastward	0.3241	7.3845	0.3399
"Nepartak"	Northward	0.6393	3.7112	0.2646
	Westward	0.3607	1.8134	0.3898
"Meari"	Northward	0.5550	3.6618	0.2410
	Westward	0.4450	0.5660	0.2584

The colour assigned to each node x_i (Figs 5, 8d and 9d) correspond to the target cluster with the highest probability P_k. Nodes with a probability lower than 1e–10 are greyed out. The boundary of colours is defined as the separatrix.

https://doi.org/10.5194/egusphere-2025-1458
Preprint. Discussion started: 14 April 2025

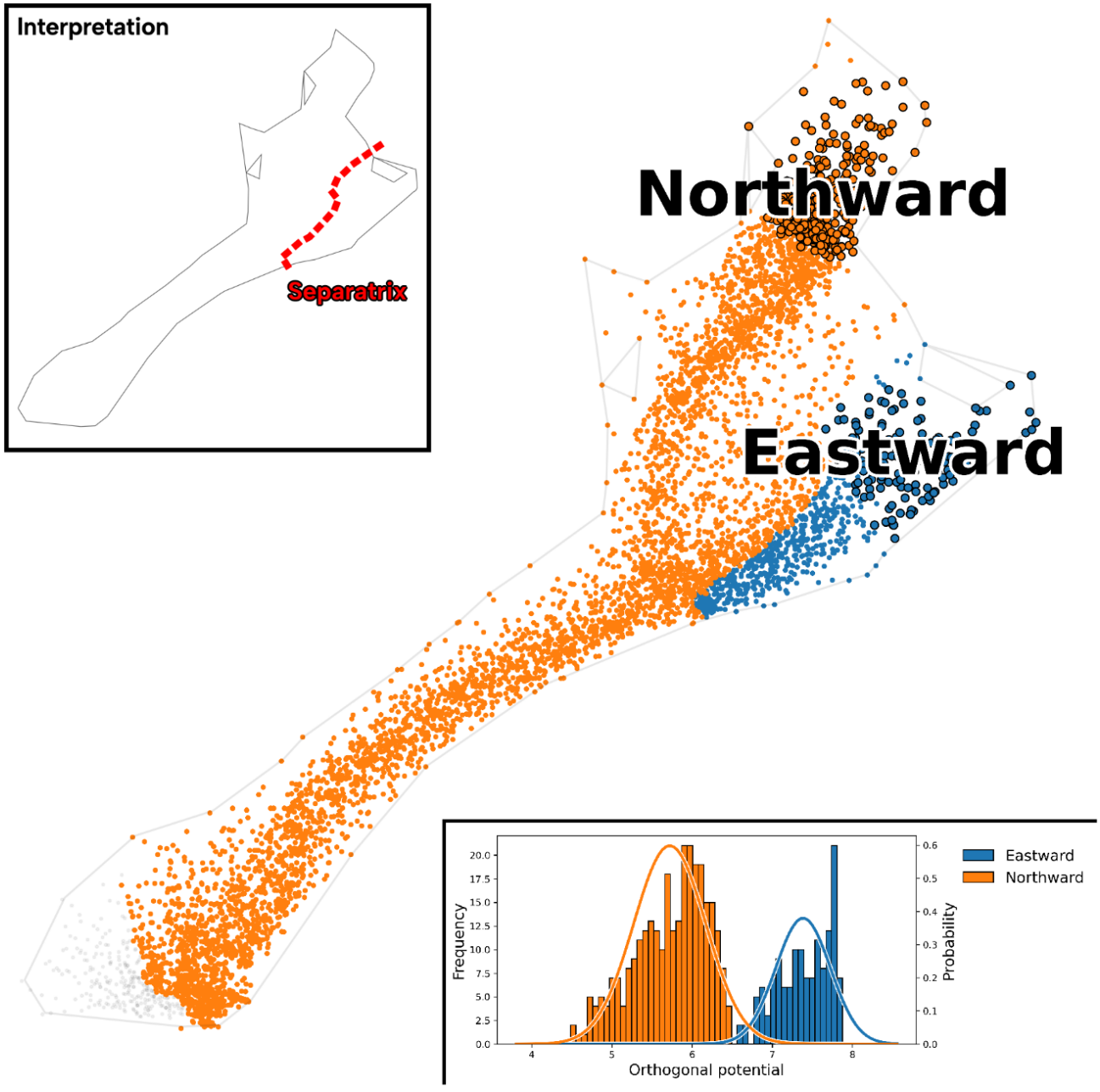

Figure 5: Dynamical clustering. The separatrix exists at the separation between orange ("Northward") and blue ("Eastward") colours. Bottom inset: Gaussian mixture of orthogonal potential. Top inset: the location of the separatrix at the colour separation.

https://doi.org/10.5194/egusphere-2025-1458
Preprint. Discussion started: 14 April 2025

2.2 Tropical cyclone tracking

To track the tropical cyclone (TC) centres, the pressure reduced at the mean sea level, the horizontal wind at 850 and 300 hPa, the wind speed at 10 m and the relative humidity at 925 hPa are used. Because it is not directly available in JMA-MEPS, the specific humidity at 925 hPa is derived from the relative humidity, the absolute temperature, and the pressure (Bolton, 1980) at the same pressure level.

The identification of TC centres is performed by combining the "Okubo-Weiss-Zeta" (OWZ) tracker (Bourdin et al., 2022; Tory et al., 2013; Ullrich and Zarzycki, 2017), the pressure centroid method (PCM; Nguyen et al., 2014) and the Hart phase space diagram (HPSD; Hart, 2003). OWZ detects the low-deformation vorticities within large-scale disturbance in the 850-hPa horizontal wind. Additionally, both the relative and specific humidity inform about the thermodynamic, while the vertical wind shear between 850 and 300 hPa gives information about the shear environment. Thresholds are applied to establish if the surrounding environment is, or not, favourable to the existence of a TC. While PCM relocates the centre into the inner core, if necessary, HPSD only retains full-troposphere warm cores. More details can be found in Oettli and Kotsuki (2024a). For the three TCs used in this study, the detection method is applied at each initialization time and for each of the ensemble members (Table 2).

Table 2: Miscellaneous characteristics. Number of ensemble members, forecast horizons and initialization times in MEPS, number of identified TC positions, and number of midpoints and their associated velocities, by tropical cyclone.

Tropical Cyclone Name	Number of Ensemble Members	Number of Forecast Horizons	Number of Initialization Times	Number of Identified Positions	Number of Midpoints and Velocities
"Dolphin"	21[a]	14	22	6468	6006
"Nepartak"	〃	〃	16	4704	4368
"Meari"	〃	〃	13	3822	3549

[a] 1 reference member + 20 perturbed members by paired singular vectors

Original tracks are first projected from the World Geodetic System 1984 to the JGD2011/UTM zone 53N system to get positions in meters, then scaled by the standard deviation in both the x and y directions (Fig. 6b), to give the same weight to both the directions. See Oettli and Kotsuki (2024a) for more details on the tropical cyclones chosen to illustrate the application of the meteorological landscape and on the data transformation.

https://doi.org/10.5194/egusphere-2025-1458
Preprint. Discussion started: 14 April 2025

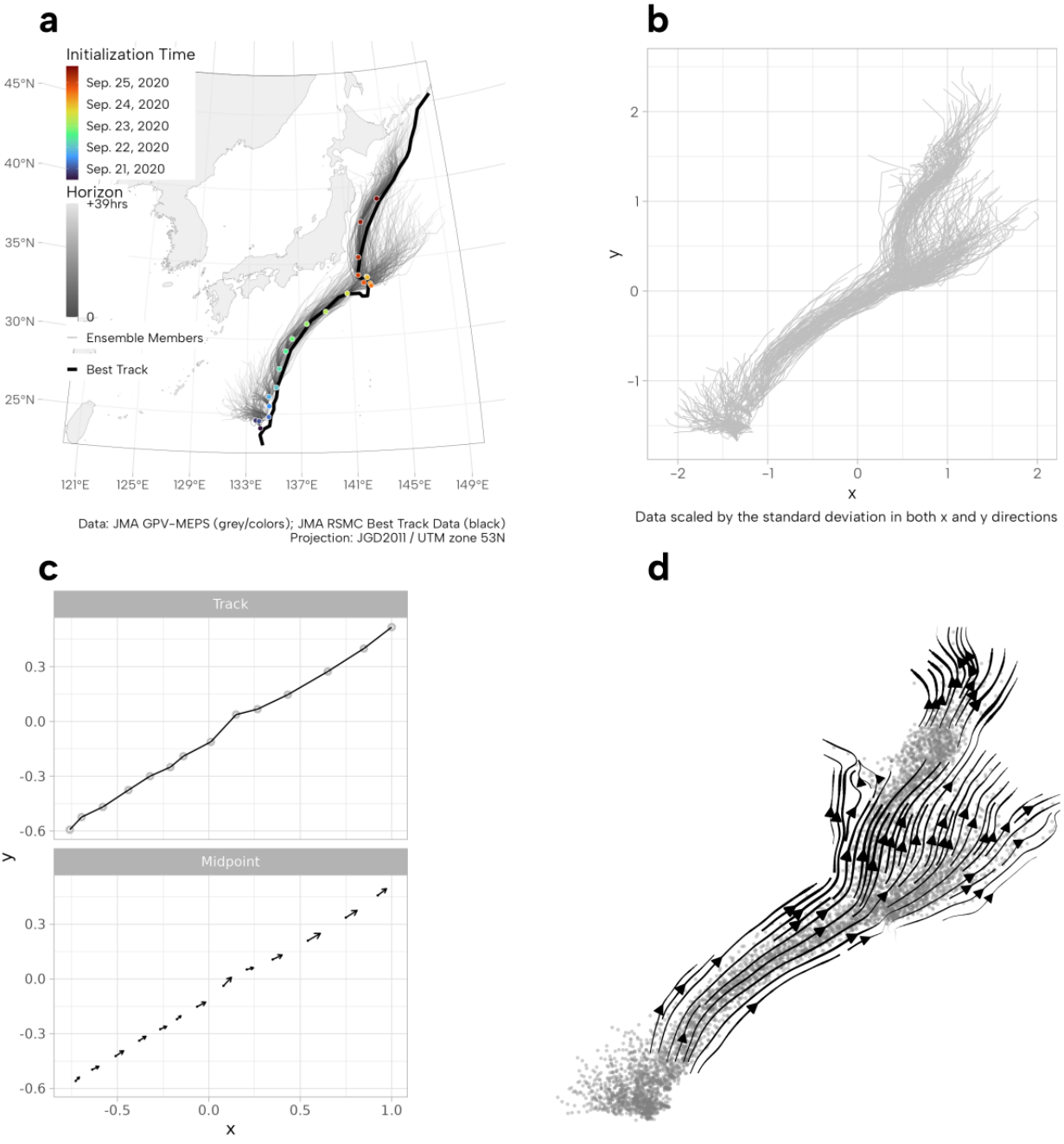

Figure 6: Input data and transformation. a) Original data, with the best track of tropical cyclone "Dolphin" (solid black line), the initial in JMA-MEPS[47] (coloured dots, each colour corresponding to an initialization time) and the forecasted tracks (lines, each gradation of grey expressing the 14 forecast horizons in hours since the initialization). The total number of ensemble members is 21. b) Transformed data by scaling the original data (in meters) by its standard deviation in x and y directions, respectively. c) The velocities (in x and y directions) are derived from the speed of the tropical centre along the tracks between two consecutive positions. The associated position is the average position between 2 consecutive positions. d) The input vector field for this study, consisting of 6006 points (grey dots) and associated velocities (streamlines with arrow).

https://doi.org/10.5194/egusphere-2025-1458
Preprint. Discussion started: 14 April 2025

3 Data

3.1 Ensemble prediction system

The Meso-scale Ensemble Prediction System (MEPS; Ono et al., 2021), operated by the Japan Meteorological Agency (JMA), provides probabilistic information and multi-scenarios based on 21 ensemble members, with 1 reference member and 20 perturbed members with initial conditions using paired singular vectors (Buizza and Palmer, 1995). JMA-MEPS supplies forecasts of common meteorological fields (e.g., horizontal wind, air temperature or geopotential height) near the surface and at different pressure levels. The prediction system is initialized 4 times a day, at 00:00:00, 06:00:00, 12:00:00 and 18:00:00 UTC, with 14 forecast horizons (every 3 hours) each up to 39 hours.

In the predicted trajectory by the EPS, for the same ensemble member and the same initialization time, the displacement between two consecutive positions of the TC centre (at two consecutive forecasting time) are extracted. The velocity vector is calculated by dividing the displacement vector between these two points by the time interval (3 hours for MEPS). This velocity vector is then assigned to the midpoint coordinates of these two points (Fig. 7c). This calculation is performed for all consecutive pairs of points contained in the trajectories of all ensemble members. The coordinates of the midpoints obtained from each calculation correspond to the nodes of the 2D point cloud X, and each node has its corresponding velocity vector (Fig. 7d). This data is used as input for MeteoScape to compute the meteorological landscape for a specific TC. See Table 2 for the total number of points by TC.

3.2 Tropical cyclones “Dolphin”, “Nepartak” and “Meari”

TC “Dolphin” (Fig. 6a; solid black line) came close to the Japanese coasts between the 25 and 29 September 2020, with a trajectory mostly north north-eastward, but also with a noticeable meandering on 24 September 2020. The abrupt change of direction of the tracks forecasted by MEPS (Fig. 6a; grey lines) as well as the spatial jump in the location of the initial positions (Fig. 6a; coloured dots) in the region of the meandering show the difficulty MEPS had to accurately forecast the trajectory of the tropical cyclone. Around the same time, there is a clear divergence of the forecast, with a group of tracks going following the trajectory of “Dolphin” before the start of the meandering, i.e., more eastward. And another group of tracks following the new northward trajectory after the change of direction has been observed. There is a clear spatial separation between the two groups of directions, which is the reason why the TC “Dolphin” is an interesting study case. Two other TCs, “Nepartak” and “Meari”, were also chosen to test our methodology. TC “Nepartak” crossed the norther part of the Honshu Island, Japan, on 28 July 2021, after a change in its trajectory occurred the day prior (Fig. 8a). TC “Meari” formed on 10 August 2022 and hit Honshu Island on 13 August 2022 (Fig. 9a).

https://doi.org/10.5194/egusphere-2025-1458
Preprint. Discussion started: 14 April 2025

4 Results

4.1 MeteoScape Leads to Meteorological Landscape and Separatrix from Ensemble Forecasting Data

Waddington's epigenetic landscape simplifies complex flow using the surface (landscape), formed by valleys and ridges, and the gradient on it represents its flow. Mathematically, Waddington's epigenetic landscape represents a potential field (gradient field) approximation of a vector field, i.e., $f = -\nabla\phi$, where f is the vector field, gradient operator ∇, and potential ϕ. The Helmholtz-Hodge decomposition (HHD; Bhatia et al., 2013; Suda, 2020) of a vector field is widely used as a method to extract the potential field. The HHD of a vector field separates its irrotational (curl-free) component $-\nabla\phi$ from its solenoidal (divergence-free) component $\nabla \times A$ (where A is the vector potential), to understand the unique properties of a flow (such as its incompressibility or vorticity). HHD is applied across various research fields, including fluid dynamics(Ribeiro et al., 2016; Sprössig, 2010), aeroacoustics (Schoder et al., 2019, 2020), oceanography (Forget and Ferreira, 2019; Li et al., 2012; Watterson, 2001), seismology (Lay and Wallace, 1995; Scott and Helmberger, 1983) or meteorology (Chen and Wiin-Nielsen, 1976; Hawkins and Rosenthal, 1965; Krishnamurti, 1968; Lorenc, 1984; Lorenz, 1960). However, HHD can only achieve high accuracy when observation points are uniformly distributed within the domain because HHD requires solving the partial differential equations using methods such as the finite element method, leading to the inappropriateness of HHD to ensemble forecast data. In addition, HHD is difficult to extend to high-dimensional cases due to the curse of dimensionality.

The graph Hodge decomposition (GHD) is the HHD applied to a weighted directed graph (Jiang et al., 2011; Johnson and Goldring, 2013; Lim, 2020; Maehara and Ohkawa, 2019) with application to economics (Fujiwara et al., 2021; Fujiwara and Islam, 2020; Iyetomi et al., 2020; Kichikawa et al., 2018), neural networks (Miura and Aoki, 2015b, a), urban planning (Aoki et al., 2022) or biology (Imoto and Hiraoka, 2023; Johnson and Goldring, 2013; Qiu et al., 2022; Yachimura et al., 2023) for example. GHD decomposes a directed graph into an acyclic-directed graph corresponding to the potential field and a divergence-free directed graph corresponding to the rotational field. GHD does not encounter the above problems of HHD because its accuracy is independent of the density of the point cloud and its computational cost is independent on dimension of data. Therefore, we developed the meteorological landscapes analysis method, MeteoScape (Fig. 1c), based on GHD.

MeteoScape constructs a weighted directed graph from point cloud and velocity data using a k-nearest neighbour algorithm and velocity embedding (Fig. 2a). Then, MeteoScape decomposes the weighted directed graph using GHD. MeteoScape retransforms the decomposed graph back into the potential and rotational flow (Fig. 3a, c). By computing the contribution rates of the potential and rotational flow for the entire flow, we can identify the essential component of flow (Fig. 3). Furthermore, MeteoScape derives an orthogonal potential from decomposed flow, with its contours representing the orbits in the flow (Fig. 3b, d). MeteoScape identifies the paths on the landscape by analysing the contours of the orthogonal potential, connecting start-point and end-point clusters (Fig. 4b). Additionally, MeteoScape performs dynamical clustering using the Gaussian mixture clustering of the orthogonal potential and identifies the separatrix that separates the fates of orbits leading to end-point clusters (Fig. 5). Details of the MeteoScape algorithm are written in Sect. 2.

https://doi.org/10.5194/egusphere-2025-1458
Preprint. Discussion started: 14 April 2025

4.2 Meteorological Landscape of Tropical Cyclone "Dolphin": A Separation Scenario

The potential component from the MeteoScape (Fig. 3a), calculated from the EPS of TC "Dolphin" in 2020, has a clear northward flow from around the central part of the figure, then north-westward and finally mostly north-eastward. A secondary eastward flow is also visible in the potential, to the right of the figure. Its orthogonal component, the development orbit (Fig. 3b), also shows the general northward direction of the flow, as shown by the equipotential lines. The flow takes place between the regions of low (bottom left) and high (top right) potentials (Fig. 7). The rotational component (Fig. 3c) is generally (anti-) clockwise in the right (left) part of the flow. Two well developed whirls are visible in the northern part of the flow, which correspond to the lowest (blueish colours) and highest (reddish colours) value of the periodic orbit (Fig. 3d). Smaller orbits can be seen in the eastern part of the surface, corresponding to the anti- and clockwise rotations in the rotational flow. For TC "Dolphin", the potential (c^{pot}) and rotational (c^{rot}) components contribute for about 61% and 39% respectively (Table 3), indicating that the track of the "Dolphin" was mainly dominated by the potential flow.

Table 3: Contribution rates c^{pot} and c^{rot} to the graph-Hodge decomposition. Percentage given for TCs "Dolphin", "Nepartak" and "Meari", respectively.

	c^{pot}(%)	c^{rot}(%)
"Dolphin"	61.08	38.92
"Nepartak"	52.88	47.12
"Meari"	57.27	42.73

https://doi.org/10.5194/egusphere-2025-1458
Preprint. Discussion started: 14 April 2025

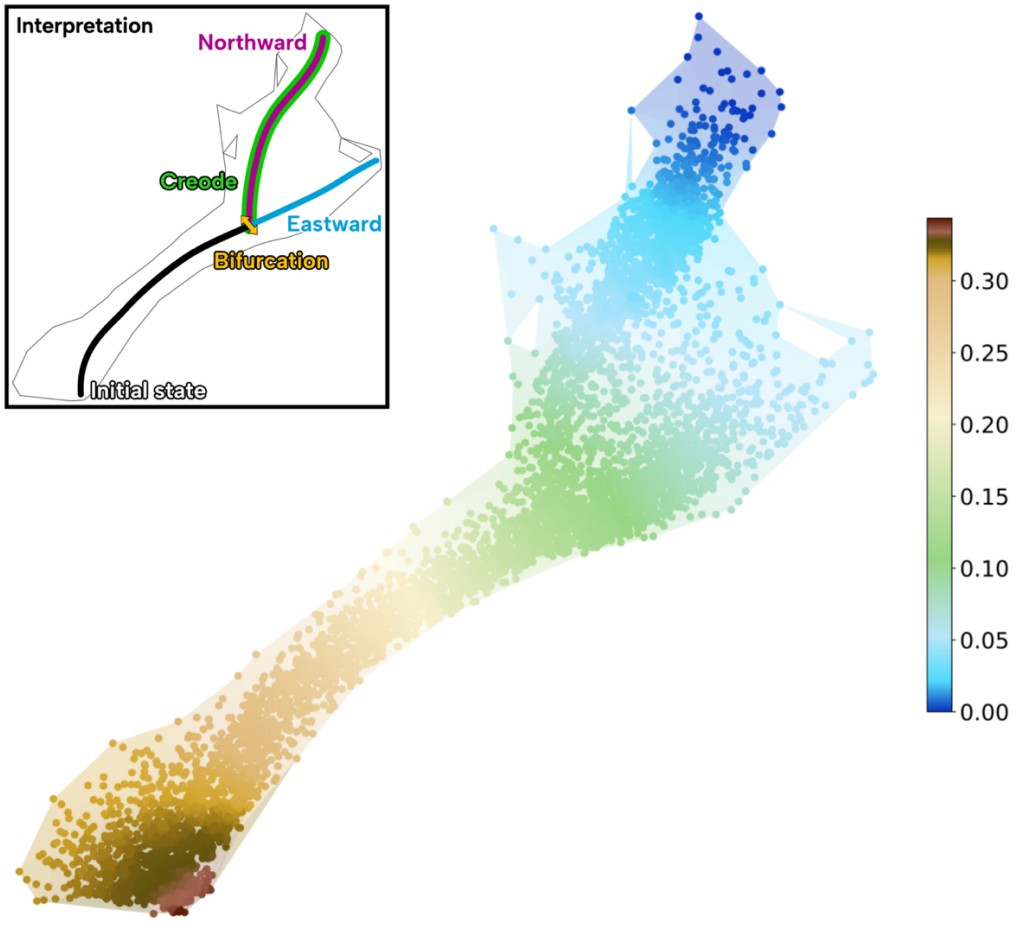

Figure 7: Hodge potential. The Hodge potential illustrates the structure of the flow from the nodes with high potential (brownish colours) to the nodes with low potential (blueish colours). Inset shows the interpretation, in a similar way than Fig. 1 a ("Interpretation").

The equivalent of the potential surface in the Waddington's landscape in the graph theory is the Hodge potential ϕ. It identifies the hierarchy of the nodes in the flow, i.e., the height of a node relative to the others. In Fig. 7, high potentials are in brownish colours, while low potentials are in blueish colours. In bioinformatics, the direction of cell differentiation can be inferred from the gradient of the Hodge potential. For example, Imoto and Hiraoka (2023) have shown that the potential can accurately represent the processes of differentiation of pancreatic endocrine cells, from pre-endocrine to mature endocrines. In the case of a TC, if ϕ at position x1 is high, then the TC at x1 has several fates, i.e., possible endpoints (or directions). In contrast, if ϕ is low, TC has only a few fates, or even a unique one.

Nodes in the southern part of the surface have the highest potential, while the nodes in the northern part have the lowest potential, representing the main direction of the flow. A secondary direction also exists from the south to the east, where

https://doi.org/10.5194/egusphere-2025-1458
Preprint. Discussion started: 14 April 2025

nodes with low values of potential (but not the lowest) can be found. Thus, there is an initial flow going northward, then going north-eastward (black line in the inset "Interpretation", Fig. 7). This is equivalent to the initial valley of the landscape, as described in Fig. 1a. Then, somewhere in the middle of the surface, a bifurcation appears between the two branches (orange left right arrow), signalling the existence of saddle point in this region. Two valleys then open (as depicted in Fig. 1a). The main flow takes the northward valley (dark magenta), to the lowest potential, while the secondary flow goes to eastward valley (strong blue). Therefore, according to Fig. 1a, a separatrix exists somewhere between the two valleys. We now focus on the detection of its precise location.

From the Hodge potential ϕ, two target clusters are defined for Northward and Eastward regimes, respectively (Fig. 4a), to represent the two valleys of the landscape. A source cluster is also defined in the region of highest potential. For this study, the source and target clusters are defined in a straightforward way. The "Start" cluster is a group of points (=TC center) chosen at the beginning of the lifetime of TC "Dolphin", without consideration for a specific initialization and/or forecast time. The "Northward" and "Eastward" clusters are composed by points taken at the end of each branch, also without considering any specific initialization and/or forecast time. We tested with diverse groups of points, but always taken in the same regions of the 2D point cloud, and it did not change the results.

Optimal trajectories (Fig. 4b) from source cluster "Start" to target cluster "Northward" (orange lines) follow the isolines of the development orbit (Fig. 3b), with a large spread of trajectories throughout the original branch (or initial valley of the Waddington's landscape as showed in Fig. 7). To the contrary of the trajectories going to the target cluster "Eastward" (blue lines) which are confined to the right border of the domain, almost following the same pathway in their first half, before diverging when arriving at the nodes composing the cluster.

The dynamical clustering (Fig. 5) uses the Gaussian mixture to assign nodes to one of the target clusters. In orange, the nodes belonging to the "Northward" cluster, and in blue, to the "Eastward" one. The nodes in light grey are not clustered as they do not play a role in the definition of optimal trajectories (Fig. 4b). The bottom inset in Fig. 5 shows the Gaussian distribution curves ("Probability"; coloured lines) and the distributions of the nodes ("Frequency"; coloured bar). The x-axis is the value of development potential (Fig. 3b) at each node. It shows a clear separation between the Gaussian distribution curve, corresponding to the boundary between the blue and orange dots in the main figure. This is also where the separatrix takes place (red dashed segment in top inset).

4.3 Tropical Cyclones "Nepartak" and "Meari": Other Separation Cases

The same methodology is applied to tropical cyclones "Nepartak" in 2021 and "Meari" in 2022, i.e., by first defining source and target clusters. Then by applying the GHD to a weighted directed graph (not shown) to calculate ϕ and draw the associated landscape. And finally, by dynamically assigning a cluster to the nodes with GMM to find the separatrix in the tracks forecasted by MEPS.

In the case of TC "Nepartak" (Fig. 8a), the landscape reconstructed from ϕ (Fig. 8b) has a general slope for the southeastern region (highest values) to the western region (lowest values) of the potential surface. A secondary region of lower values is

https://doi.org/10.5194/egusphere-2025-1458
Preprint. Discussion started: 14 April 2025

also visible in the northern part of the surface. Accordingly, two target clusters ("Westward" and "Northward") are defined (Fig. 8c), with both being quite close to each other, because of the general shape of the potential surface. The clustering of the nodes from the GMM (Fig. 8e) exhibits a clear separation (i.e., the separatrix) between the blue and orange dots (Fig. 8d).

https://doi.org/10.5194/egusphere-2025-1458
Preprint. Discussion started: 14 April 2025

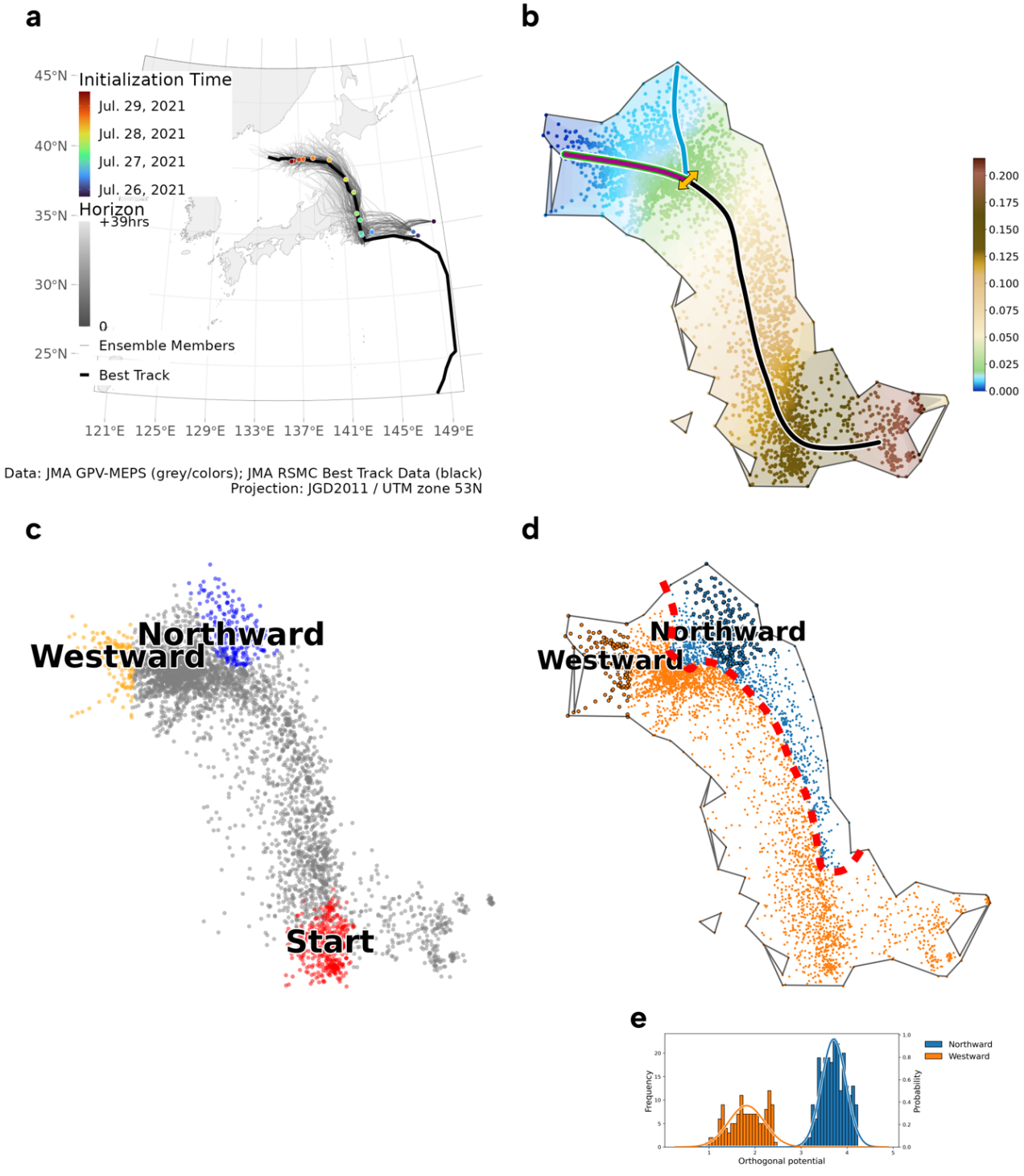

Figure 8: Tropical cyclone "Nepartak". a) Original data, b) Hodge potential, c) clusters, d) dynamical clustering and e) Gaussian mixture.

https://doi.org/10.5194/egusphere-2025-1458
Preprint. Discussion started: 14 April 2025

For TC “Meari” (Fig. 9a), the main slope of the landscape (Fig. 9b) follows a curve to the left, from the highest values in the southeastern region to the lowest values in the northern region. A secondary slope also appears, exiting to the west. Two clusters, “Westward” and “Northward”, are thus created (Fig. 9c) and the clustering of the nodes applied to obtain the GMM (Fig. 9e) and the associated dynamical clustering (Fig. 9d). In this case, a separatrix appears at the boundary between blue and orange dots. This separatrix corresponds to the separation between the Gaussian curves in the GMM.

https://doi.org/10.5194/egusphere-2025-1458
Preprint. Discussion started: 14 April 2025

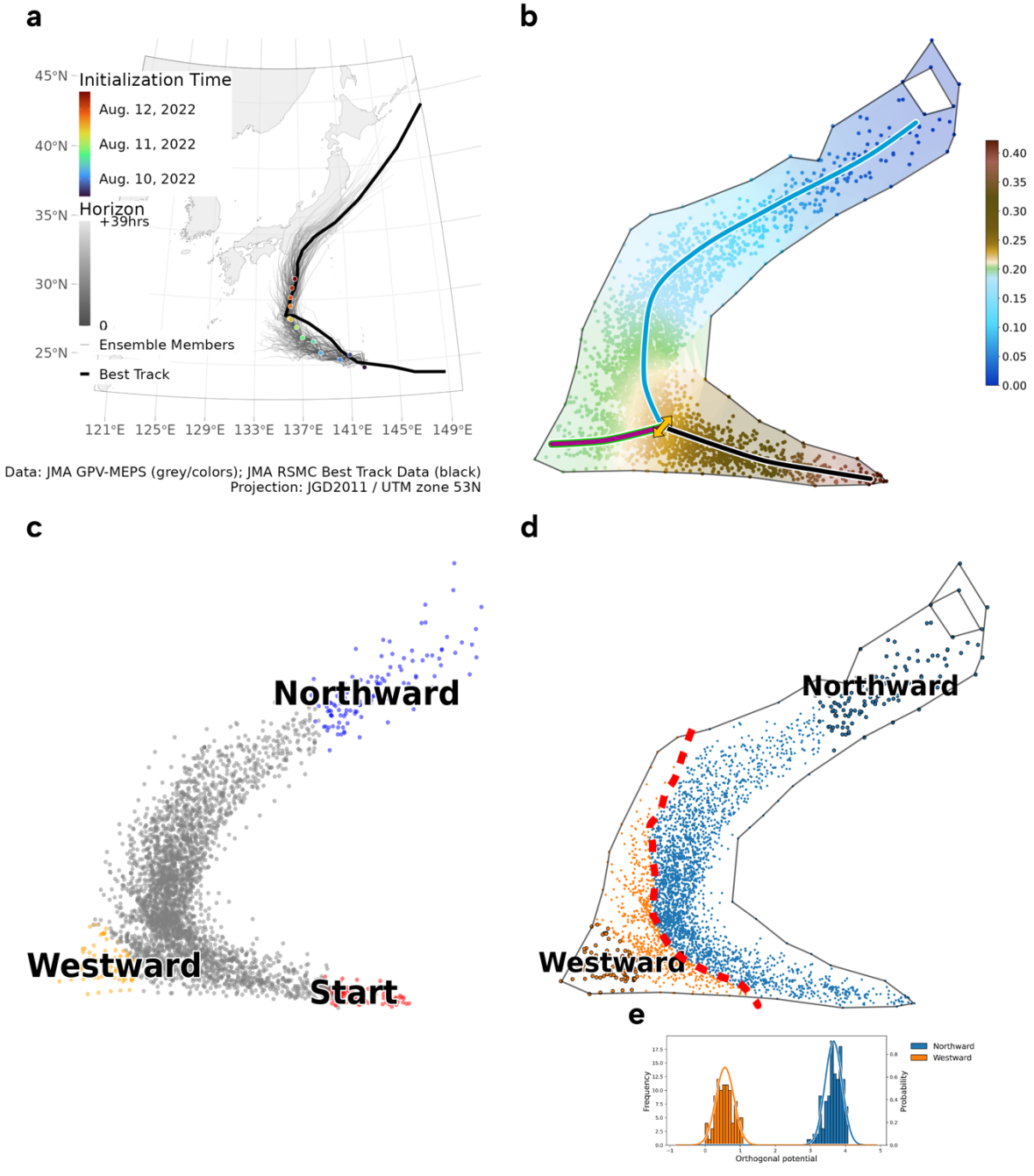

Figure 9: Same as Fig. 8 but for tropical cyclone "Meari".

The contribution rates for TCs "Nepartak" and "Meari" are equivalent to those found for "Dolphin" (Table 3), with the potential flow dominating the rotational flow. However, in the case of TC "Nepartak," the contribution rates are almost

https://doi.org/10.5194/egusphere-2025-1458
Preprint. Discussion started: 14 April 2025

equivalent. It is not clear why, but a possible explanation would be the way the contributions are calculated, because there is no unique method to define the contribution rates for a vector field.

5 Conclusions

In this study, we have successfully applied mathematical methods developed in bioinformatics to meteorology. Applying these methods to the positions of three tropical cyclones forecasted by an ensemble prediction system, we have been able to calculate the Hodge potential ϕ, via the graph Hodge decomposition, to illustrate the surface of the meteorological landscape. Then, by analyzing the shape of this landscape, we detected the major paths of evolution of the tropical cyclones. Finally, by the dynamical clustering using the orthogonal potential and Gaussian mixture model, we were able to locate a separatrix in the potential surface, mathematically separating the major paths previously identified. Chaotic dynamics are known to have infinite-dimensional attractors with bifurcations like Lorenz's butterfly. Therefore, having pathways separated by separatrix for TCs is natural because the atmosphere is also a chaotic system. Identifying the possible scenarios of TCs would help to reduce both the human and economic costs. In the case of a separation into a threatening/non-threatening trajectory, as illustrated in this study, detecting such scenario may help to activate (or not) mitigation measures and, more generally, to improve the preparedness.

The description of the meteorological landscape has been done here for a two-dimensional case (i.e., a tropical cyclone centre), but it also can be done for higher-dimensional weather events, such as heavy rains. It first requires a mapping of the multidimensional space into a 3-dimensional space, through dimension reduction techniques (Imoto and Hiraoka, 2023), such as the Principal Component Analysis (PCA), the Uniform Manifold Approximation and Projection (UMAP) or the Non-negative Matrix Factorization (NMF), among others.

MEPS only has 21 ensemble members (1 unperturbed and 20 perturbed by paired singular vectors). However, the limited number of perturbed members can limit the measurement of uncertainty for certain types of weather events (Buizza and Palmer, 1995). Increasing the number of ensemble members, with the help of large-ensemble prediction systems, could be beneficial (Kondo and Miyoshi, 2019; Leutbecher, 2019), for example to evaluate the stability of the mathematical methods with more information available. However, we could quickly reach a computational bottleneck because the calculation of ϕ requires the Moore–Penrose pseudoinverse of the graph Laplacian, which computational cost increases with the size of the matrix (the number of point cloud).

Another current limitation is the necessity to know all the positions of a tropical cyclone to draw the meteorological landscape. A future task would be to find a way to recalculate the Hodge potential at each new forecast, while keeping track of the calculations during the previous forecast in the calculation, to ensure a smooth continuity in the landscape. Also, we need to confirm that the detection of separatrix also works when there is no separatrix, which could occur when the ensemble members agree.

https://doi.org/10.5194/egusphere-2025-1458
Preprint. Discussion started: 14 April 2025

Also, MEPS skills have not been evaluated prior to its use in the present study. Particularly, the track errors have not been assessed. However, we believe that errors in the tropical cyclone's position are not a major concern for this study, because we are more interested in the evolution of the forecasts in time, with their respective errors, to depict the meteorological Waddington's landscape. We are presenting proof of concept and how it can be used in meteorology.

Code and data availability

MeteoScape is archived on Zenodo under 10.5281/zenodo.15122828 (Oettli et al., 2025) with a MIT license. Scripts to produce the different figures of MeteoScape are written in Python (v3.11.5 van Rossum, 1995; van Rossum and Drake, 2009), with the help of package "Matplotlib" (Hunter, 2007). Data are available on Zenodo under 10.5281/zenodo.11064128 (Oettli and Kotsuki, 2024b) with a CC BY 4.0 license, in NetCDF format (Brown et al., 1993; Rew and Davis, 1990). Data have been read, processed, and formatted using the R project for statistical computing (v4.3.3; R Core Team, 2023), with the help of packages "metR" (Campitelli, 2021), "sf" (Pebesma, 2018; Pebesma and Bivand, 2023) and "anndata" (Cannoodt, 2023). MeteoScape is based on CellMap (Imoto, 2023), a ribonucleic acid (RNA) landscape inference method.

Author contribution

S.K. designed and directed the project; K.T. conceived the original idea; Y.I. developed the computational framework; P.O. performed the calculations and designed the figures. P.O. and Y.I. wrote the manuscript with input from K.T and S.K. All authors discussed the results and contributed to the final manuscript.

Competing interests

The authors declare that they have no conflict of interest.

Acknowledgments

This work was performed under the auspices of the Moonshot Research and Development Program of the Japan Science and Technology Agency, the Japan Society for the Promotion of Science and the IAAR Research Support Program of Chiba University. Authors are also grateful to the Japan Meteorological Agency for operating the MEPS data.

Financial support

This research has been supported by the Japan Science and Technology Agency (JST) through the Moonshot Research and Development Program (grants JPMJMS2284 and JPMJMS2389), the Japan Society for the Promotion of Science (JSPS)

https://doi.org/10.5194/egusphere-2025-1458
Preprint. Discussion started: 14 April 2025

KAKENHI (grants JP21H04571 and JP22K18821). Y.I. has been supported by JST (grants JPMJPR2021, JPMJFR222X, and JPMJCR24Q1).

References

Aoki, T., Fujishima, S., and Fujiwara, N.: Urban spatial structures from human flow by Hodge–Kodaira decomposition, Sci. Rep., 12, 11258, https://doi.org/10.1038/s41598-022-15512-z, 2022.

Bentley, J. L.: Multidimensional binary search trees used for associative searching, Commun. ACM, 18, 509–517, https://doi.org/10.1145/361002.361007, 1975.

Bhatia, H., Norgard, G., Pascucci, V., and Bremer, P.-T.: The Helmholtz-Hodge decomposition—A survey, IEEE Trans. Vis. Comput. Graph., 19, 1386–1404, https://doi.org/10.1109/TVCG.2012.316, 2013.

Bolton, D.: The computation of equivalent potential temperature, Mon. Wea. Rev., 108, 1046–1053, https://doi.org/10.1175/1520-0493(1980)108<1046:TCOEPT>2.0.CO;2, 1980.

Bourdin, S., Fromang, S., Dulac, W., Cattiaux, J., and Chauvin, F.: Intercomparison of four algorithms for detecting tropical cyclones using ERA5, Geosci. Model Dev., 15, 6759–6786, https://doi.org/10.5194/gmd-15-6759-2022, 2022.

Brown, S. A., Folk, M., Goucher, G., Rew, R., and Dubois, P. F.: Software for portable scientific data management, Comput. Phys., 7, 304–308, https://doi.org/10.1063/1.4823180, 1993.

Buizza, R. and Palmer, T. N.: The singular-vector structure of the atmospheric global circulation, J. Atmos. Sci., 52, 1434–1456, https://doi.org/10.1175/1520-0469(1995)052<1434:TSVSOT>2.0.CO;2, 1995.

Campitelli, E.: metR: tools for easier analysis of meteorological fields, https://doi.org/10.5281/zenodo.2593516, 2021.

Cannoodt, R.: anndata: “anndata” for R, https://doi.org/10.32614/CRAN.package.anndata, 2023.

Chen, T.-C. and Wiin-Nielsen, A. C.: On the kinetic energy of the divergent and nondivergent flow in the atmosphere, Tellus, 28, 486–498, https://doi.org/10.1111/j.2153-3490.1976.tb00697.x, 1976.

Dijkstra, E. W.: A note on two problems in connexion with graphs, Numer. Math., 1, 269–271, https://doi.org/10.1007/BF01386390, 1959.

Eppstein, D., Paterson, M. S., and Yao, F. F.: On nearest-neighbor graphs, Discrete Comput. Geom., 17, 263–282, https://doi.org/10.1007/PL00009293, 1997.

Ferrell, J. E., Jr.: Bistability, bifurcations, and Waddington’s epigenetic landscape, Curr. Biol., 22, R458–R466, https://doi.org/10.1016/j.cub.2012.03.045, 2012.

Forget, G. and Ferreira, D.: Global ocean heat transport dominated by heat export from the tropical Pacific, Nat. Geosci., 12, 351–354, https://doi.org/10.1038/s41561-019-0333-7, 2019.

Fujiwara, Y. and Islam, R.: Hodge decomposition of Bitcoin money flow, in: Advanced studies of financial technologies and cryptocurrency markets, edited by: Pichl, L., Eom, C., Scalas, E., and Kaizoji, T., Springer, Singapore, 117–137, 2020.

https://doi.org/10.5194/egusphere-2025-1458
Preprint. Discussion started: 14 April 2025

Fujiwara, Y., Inoue, H., Yamaguchi, T., Aoyama, H., Tanaka, T., and Kikuchi, K.: Money flow network among firms' accounts in a regional bank of Japan, EPJ Data Sci., 10, 1–26, https://doi.org/10.1140/epjds/s13688-021-00274-x, 2021.

Gilbert, S. F.: Epigenetic landscaping: Waddington's use of cell fate bifurcation diagrams, Biol. Philos., 6, 135–154, https://doi.org/10.1007/BF02426835, 1991.

Hart, R. E.: A cyclone phase space derived from thermal wind and thermal asymmetry, Mon. Wea. Rev., 131, 585–616, https://doi.org/10.1175/1520-0493(2003)131<0585:ACPSDF>2.0.CO;2, 2003.

Hawkins, H. F. and Rosenthal, S. L.: On the computation of stream functions from the wind field, Mon. Wea. Rev., 93, 245–252, https://doi.org/10.1175/1520-0493(1965)093<0245:OTCOSF>2.3.CO;2, 1965.

Hunter, J. D.: Matplotlib: A 2D Graphics Environment, Comput. Sci. Eng., 9, 90–95, https://doi.org/10.1109/MCSE.2007.55, 2007.

Imoto, Y.: CellMap - RNA landscape inference method, GitHub [code] https://github.com/yusuke-imoto-lab/CellMap, 2023.

Imoto, Y. and Hiraoka, Y.: V-Mapper: topological data analysis for high-dimensional data with velocity, Nonlinear Theory Its Appl. IEICE, 14, 92–105, https://doi.org/10.1587/nolta.14.92, 2023.

Iyetomi, H., Aoyama, H., Fujiwara, Y., Souma, W., Vodenska, I., and Yoshikawa, H.: Relationship between macroeconomic indicators and economic cycles in U.S., Sci. Rep., 10, 8420, https://doi.org/10.1038/s41598-020-65002-3, 2020.

Jiang, X., Lim, L.-H., Yao, Y., and Ye, Y.: Statistical ranking and combinatorial Hodge theory, Math. Program., 127, 203–244, https://doi.org/10.1007/s10107-010-0419-x, 2011.

JMA: Status and issues of current numerical forecast models in the Japan Meteorological Agency, 1st Numerical Forecast Model Development Roundtable, Tokyo, Japan, 1–26, 2017.

Johnson, J. L. and Goldring, T.: Discrete Hodge theory on graphs: a tutorial, Comput. Sci. Eng., 15, 42–55, https://doi.org/10.1109/MCSE.2012.91, 2013.

Kichikawa, Y., Iyetomi, H., Iino, T., and Inoue, H.: Hierarchical and circular flow structure of interfirm transaction networks in Japan, SSRN [preprint], ssrn:3173955, 4 May 2018.

Kondo, K. and Miyoshi, T.: Non-Gaussian statistics in global atmospheric dynamics: a study with a 10 240-member ensemble Kalman filter using an intermediate atmospheric general circulation model, Nonlin. Processes Geophys., 26, 211–225, https://doi.org/10.5194/npg-26-211-2019, 2019.

Kowaleski, A. M. and Evans, J. L.: Use of multiensemble track clustering to inform medium-range tropical cyclone forecasts, Weather Forecast., 35, 1407–1426, https://doi.org/10.1175/WAF-D-20-0003.1, 2020.

Krishnamurti, T. N.: A diagnostic balance model for studies of weather systems of low and high latitudes, Rossby number less than 1, Mon. Wea. Rev., 96, 197–207, https://doi.org/10.1175/1520-0493(1968)096<0197:ADBMFS>2.0.CO;2, 1968.

Lay, T. and Wallace, T. C.: Modern global seismology, Academic Press, San Diego, 521 pp., 1995.

Leutbecher, M.: Ensemble size: how suboptimal is less than infinity?, Q. J. R. Meteorol. Soc., 145, 107–128, https://doi.org/10.1002/qj.3387, 2019.

https://doi.org/10.5194/egusphere-2025-1458
Preprint. Discussion started: 14 April 2025

Leutbecher, M. and Palmer, T. N.: Ensemble forecasting, J. Comput. Phys., 227, 3515–3539, https://doi.org/10.1016/j.jcp.2007.02.014, 2008.

Li, A., Zhang, L., Zang, Z., and Zhang, Y.: Iterative and adjusting method for computing stream function and velocity potential in limited domains and convergence analysis, Appl. Math. Mech.-Engl. Ed., 33, 687–700, https://doi.org/10.1007/s10483-012-1580-9, 2012.

Lim, L.-H.: Hodge Laplacians on graphs, SIAM Rev., 62, 685–715, https://doi.org/10.1137/18M1223101, 2020.

Lorenc, A. C.: The evolution of planetary-scale 200 mb divergent flow during the FGGE year, Q. J. R. Meteorol. Soc., 110, 427–441, https://doi.org/10.1002/qj.49711046408, 1984.

Lorenz, E. N.: Energy and numerical weather prediction, Tellus, 12, 364–373, https://doi.org/10.1111/j.2153-3490.1960.tb01323.x, 1960.

Maehara, K. and Ohkawa, Y.: Modeling latent flows on single-cell data using the Hodge decomposition, bioRxiv [preprint], bioRxiv:592089, 28 March 2019.

Miura, K. and Aoki, T.: Hodge–Kodaira decomposition of evolving neural networks, Neural Netw., 62, 20–24, https://doi.org/10.1016/j.neunet.2014.05.021, 2015a.

Miura, K. and Aoki, T.: Scaling of Hodge-Kodaira decomposition distinguishes learning rules of neural networks, IFAC-Pap., 48, 175–180, https://doi.org/10.1016/j.ifacol.2015.11.032, 2015b.

National Centers for Environmental Prediction/National Weather Service/NOAA/U.S. Department of Commerce, Japan Meteorological Agency/Japan, Met Office/Ministry of Defence/United Kingdom, China Meteorological Administration/China, Meteorological Service of Canada/Environment Canada, Korea Meteorological Administration/Republic of Korea, Meteo-France/France, European Centre for Medium-Range Weather Forecasts, and Bureau of Meteorology/Australia: THORPEX interactive grand global ensemble (TIGGE) model tropical cyclone track data, Research Data Archive at the National Center for Atmospheric Research, Computational and Information Systems Laboratory [data set], https://doi.org/10.5065/D6GH9GSZ, 2008.

Nguyen, L. T., Molinari, J., and Thomas, D.: Evaluation of tropical cyclone center identification methods in numerical models, Mon. Wea. Rev., 142, 4326–4339, https://doi.org/10.1175/MWR-D-14-00044.1, 2014.

Nishimura, M. and Yamaguchi, M.: Selective ensemble mean technique for tropical cyclone track forecasts using multi-model ensembles, Trop. Cyclone Res. Rev., 4, 71–78, https://doi.org/10.6057/2015TCRR02.03, 2015.

Oettli, P. and Kotsuki, S.: An objective detection of separation scenario in tropical cyclone trajectories based on ensemble weather forecast data, J. Geophys. Res. Atmos., 129, e2024JD040830, https://doi.org/10.1029/2024JD040830, 2024a.

Oettli, P. and Kotsuki, S.: An objective detection of separation scenario in tropical cyclone trajectories based on ensemble weather forecast data, Zenodo [data set], https://doi.org/10.5281/zenodo.11064128, 2024b.

Oettli, P., Tokuda, K., Imoto, Y., and Kotsuki, S.: MeteoScape: a meteorological landscape, Zenodo [code], https://doi.org/10.5281/zenodo.15122828, 2025.

Ono, K., Kunii, M., and Honda, Y.: The regional model-based Mesoscale Ensemble Prediction System, MEPS, at the Japan Meteorological Agency, Q. J. R. Meteorol. Soc., 147, 465–484, https://doi.org/10.1002/qj.3928, 2021.

https://doi.org/10.5194/egusphere-2025-1458
Preprint. Discussion started: 14 April 2025

Pebesma, E.: Simple features for R: standardized support for spatial vector data, The R Journal, 10, 439–446, https://doi.org/10.32614/RJ-2018-009, 2018.

Pebesma, E. and Bivand, R.: Spatial data science: with applications in R, Chapman and Hall/CRC, New York, 314 pp., 2023.

Qiu, X., Zhang, Y., Martin-Rufino, J. D., Weng, C., Hosseinzadeh, S., Yang, D., Pogson, A. N., Hein, M. Y., Min, K. H. (Joseph), Wang, L., Grody, E. I., Shurtleff, M. J., Yuan, R., Xu, S., Ma, Y., Replogle, J. M., Lander, E. S., Darmanis, S., Bahar, I., Sankaran, V. G., Xing, J., and Weissman, J. S.: Mapping transcriptomic vector fields of single cells, Cell, 185, 690-711.e45, https://doi.org/10.1016/j.cell.2021.12.045, 2022.

R Core Team: R: a language and environment for statistical computing, R Foundation for Statistical Computing, Vienna, Austria, 2023.

Rew, R. and Davis, G.: NetCDF: an interface for scientific data access, IEEE Comput. Graph. Appl., 10, 76–82, https://doi.org/10.1109/38.56302, 1990.

Ribeiro, P. C., de Campos Velho, H. F., and Lopes, H.: Helmholtz–Hodge decomposition and the analysis of 2D vector field ensembles, Comput. Graph., 55, 80–96, https://doi.org/10.1016/j.cag.2016.01.001, 2016.

Rossi, C., Madl, P., Foletti, A., and Mocenni, C.: Equilibrium and far-from equilibrium states, in: Fields of the cells, edited by: Fels, D., Cifra, M., and Scholkmann, F., Research Signpost, Trivandrum, Kerala (India), 71–94, 2015.

van Rossum, G.: Python tutorial, Centrum voor Wiskunde en Informatica (CWI), Amsterdam, 65 pp., 1995.

van Rossum, G. and Drake, F. L.: Python 3 Reference Manual, CreateSpace, Scotts Valley, CA, 242 pp., 2009.

Schoder, S., Kaltenbacher, M., and Roppert, K.: Helmholtz's decomposition applied to aeroacoustics, in: AIAA Meeting Paper, 25th AIAA/CEAS Aeroacoustics Conference, Delft, The Netherlands, 1–11, https://doi.org/10.2514/6.2019-2561, 2019.

Schoder, S., Roppert, K., and Kaltenbacher, M.: Helmholtz's decomposition for compressible flows and its application to computational aeroacoustics, SN Partial Differ. Equ. Appl., 1, 46, https://doi.org/10.1007/s42985-020-00044-w, 2020.

Scott, P. and Helmberger, D.: Applications of the Kirchhoff-Helmholtz integral to problems in seismology, Geophys. J. Int., 72, 237–254, https://doi.org/10.1111/j.1365-246X.1983.tb02815.x, 1983.

Slack, J. M. W.: Conrad Hal Waddington: the last Renaissance biologist?, Nat. Rev. Genet., 3, 889–895, https://doi.org/10.1038/nrg933, 2002.

Sprössig, W.: On Helmholtz decompositions and their generalizations—An overview, Math. Methods Appl. Sci., 33, 374–383, https://doi.org/10.1002/mma.1212, 2010.

Suda, T.: Application of Helmholtz–Hodge decomposition to the study of certain vector fields, J. Phys. A: Math. Theor., 53, 375703, https://doi.org/10.1088/1751-8121/aba657, 2020.

Thom, R.: Structural stability and morphogenesis: an outline of a general theory of models, 1st English ed., W. A. Benjamin, Reading, Massachusetts, 348 pp., 1975.

Tory, K. J., Chand, S. S., Dare, R. A., and McBride, J. L.: The development and assessment of a model-, grid-, and basin-independent tropical cyclone detection scheme, J. Clim., 26, 5493–5507, https://doi.org/10.1175/JCLI-D-12-00510.1, 2013.

https://doi.org/10.5194/egusphere-2025-1458
Preprint. Discussion started: 14 April 2025

Ullrich, P. A. and Zarzycki, C. M.: TempestExtremes: a framework for scale-insensitive pointwise feature tracking on unstructured grids, Geosci. Model Dev., 10, 1069–1090, https://doi.org/10.5194/gmd-10-1069-2017, 2017.

Waddington, C. H.: The cybernetics of development, in: The strategy of the genes, Routledge, London (UK), 11–58, https://doi.org/10.4324/9781315765471, 1957.

Watterson, I. G.: Decomposition of global ocean currents using a simple iterative method, J. Atmos. Oceanic Technol., 18, 691–703, https://doi.org/10.1175/1520-0426(2001)018<0691:DOGOCU>2.0.CO;2, 2001.

WMO: WMO atlas of mortality and economic losses from weather, climate and water extremes (1970–2019), World Meteorological Organization, Geneva, 90 pp., 2021.

Yachimura, T., Wang, H., Imoto, Y., Yoshida, M., Tasaki, S., Kojima, Y., Yabuta, Y., Saitou, M., and Hiraoka, Y.: scEGOT: Single-cell trajectory inference framework based on entropic Gaussian mixture optimal transport, https://doi.org/10.1101/2023.09.11.557102, 14 September 2023.